nature communications

Article

https://doi.org/10.1038/s41467-024-50743-w

Nickel-catalyzed regiodivergent hydrosilylation of α-(fluoroalkyl)styrenes without defluorination

Received: 10 December 2022

Accepted: 22 July 2024

Published online: 28 July 2024

Check for updates

Dachang Bai[1,2] ✉, Kangbao Zhong[1], Lingna Chang[1], Yan Qiao[3], Fen Wu[1], Guiqing Xu[1] & Junbiao Chang[1] ✉

The fluoroalkyl-containing organic molecules are widely used in drug discovery and material science. Herein, we report ligand regulated nickel(0)-catalyzed regiodivergent hydrosilylation of α-(fluoroalkyl)styrenes without defluorination, providing an atom- and step-economical synthesis route of two types of fluoroalkyl substituted silanes with exclusive regioselectivity. The *anti*-Markovnikov addition products (β-fluoroalkyl substituted silanes) are formed with monodentate phosphine ligand. Noteworthy, the bidentate phosphine ligand promote the generation of the more challenging Markovnikov products (α-fluoroalkyl substituted silanes) with tetrasubstituted saturated carbon centers. This protocol features with easy available starting materials and commercially available nickel catalysis, a wide range of substrates and excellent regioselectivity. The structure divergent products undergo a variety of transformations. Comprehensive mechanistic studies including the inverse kinetic isotope effects demonstrate the regioselectivity controlled by ligand structure through α-CF_3 nickel intermediate. DFT calculations reveal a distinctive mechanism involving an open-shell singlet state, which is crucial for generating intricate *tetra*-substituted Markovnikov products.

Organofluorine compounds have found extensive applications in the area of pharmaceuticals, agrochemicals, and materials science[1–4]. The incorporation of fluoroalkyl group, particularly the trifluoromethyl group (CF_3) into small organic molecules has a privileged role in drug development and agrochemical industry, which could improve its lipophilicity metabolic stability and bioacitivity[1–6]. However, compared to the well-developed C(sp^2)–CF_3 and C(sp)–CF_3 bonds formation[7–17], the construction of C(sp^3)–CF_3 bond with transition-metal catalysis still lags behind[18–23]. Specifically, the efficient and economical synthesis of products with tetrasubstituted carbon centers, which contain C(sp^3)–CF_3 bonds, is still highly desirable and remains a formidable challenge. One attractive strategy for the synthesis of alkyl-CF_3 compounds would be the direct transformation of α-CF_3 transition-metal intermediates, but much more challenging due to the thermodynamically favored β-F elimination[18–20].

Recently, significant advancements have been made by using the α-(trifluoromethyl)styrenes to synthesize high-value fluorinated organic compounds[24–26]. While, most of these reports focus on the formation of *gem*-difluoroalkenes and their derivatives via C–F bond cleavage (Fig. 1A)[27]. In the last few years, very limited examples to give CF_3-containing products using transition-metal catalysts. These include the carbene insertion (Rh or Fe complex), cycloaddition (Pd catalysis), or hydroboration processes (Co or Ir catalysis)[28–33]. The transformation of α-(trifluoromethyl)styrenes through α-CF_3 transition-metal intermediate

[1]State Key Laboratory of Antiviral Drugs, NMPA Key Laboratory for Research and Evaluation of Innovative Drug, School of Chemistry and Chemical Engineering, Henan Normal University, Pingyuan laboratory, Xinxiang 453007, China. [2]State Key Laboratory of Organometallic Chemistry, Shanghai Institute of Organic Chemistry, Chinese Academy of Sciences, Shanghai 200032, P R China. [3]School of Basic Medicine, Zhengzhou University, Zhengzhou 450001, P R China. ✉e-mail: baidachang@htu.edu.cn; changjunbiao@zzu.edu.cn

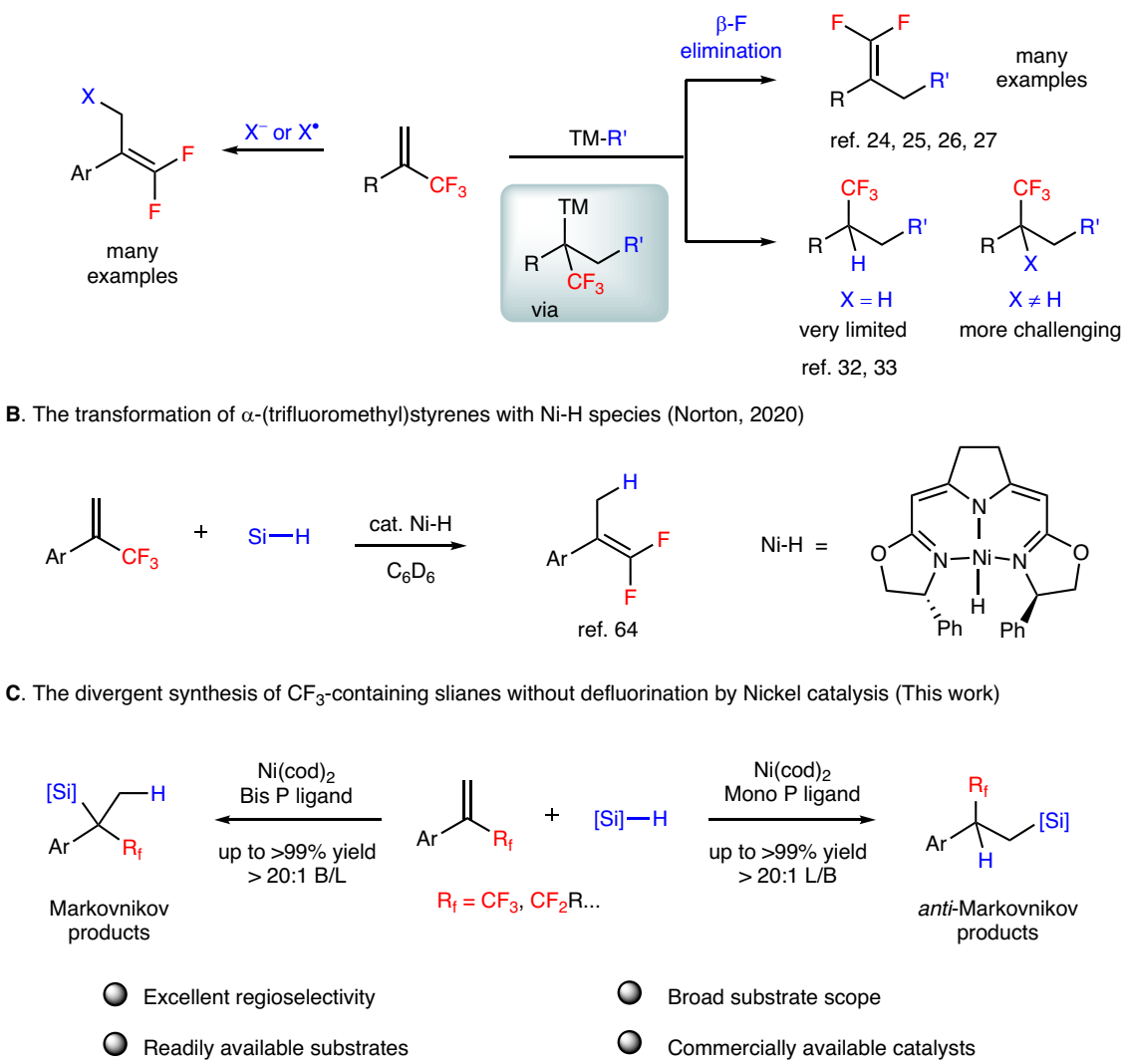

Fig. 1 | The transformation of α-(trifluoromethyl)styrenes by transition-metal catalysis. A Previous strategies for the transformation of α-(trifluoromethyl)styrenes. **B** The transformation of α-(trifluoromethyl)styrenes with Ni-H species. **C** The divergent synthesis of CF_3-containing silanes without defluorination by Nickel catalysis.

to give alkyl-CF_3 compounds is still extremely rare and remains elusive for the construction of tetrasubstituted carbon centers.

On the other hand, the transition-metal catalyzed hydrosilylation of alkenes is an atom-economic and appealing approach for the preparation of organosilanes, which find broad applications in materials science and medicinal chemistry[34–37]. Compared to the noble-metal catalysts (such as Pt, Rh, and Pd), the inexpensive and Earth-abundant first-row catalysts (such as Fe, Co, and Ni) have gained great attention over the past few dacades[38–50]. When terminal alkenes were used in these reactions, the regio control to deliver Markovnikov or anti-Markovnikov addition products is one of the most important issues[51–60]. The regiodivergent hydrosilylation would be a practical tool for the rapid construction of value-added organosilanes. In 2022, the Lu group developed a Co-catalyzed regiodivergent hydrosilylation of in situ generated α-substituted vinylsilanes for the synthesis of vicinal and geminal bis(silane)s[61]. With nickel catalysis, linear products were usually favorable, especially for the low reactive 1, 1-disubstituted alkenes[45–50,62,63]. In 2020, the Norton group reported the insertion of pincer ligated Ni(II)-H species to α-(trifluoromethyl)styrenes with silanes, only delivering the *gem*-difluoroalkene products through the β-F elimination process (Fig. 1B)[64]. Herein, we report the ligand-controlled Ni(0)-catalyzed regiodivergent hydrosilylation of α-(fluoroalkyl)styrenes with silanes, enabling the synthesis of two types of fluoroalkylsilanes with excellent regioselectivity. The anti-Markovnikov addition products were formed with monodentate phosphine ligand. In contrast, the bidentate phosphine ligand promoted the Markovnikov products with α-fluoroalkyl-containing tetrasubstituted saturated carbon centers (Fig. 1C). The trifluoromethyl group is similar in size to an isopropyl group and distinct from other alkyl group[65,66]. So, to overcome the steric hindrance of the trifluoromethyl group and avoid the β-fluorine elimination would be the two key challenges, especially for tetrasubstituted carbon center formation.

Results and discussion

Reaction investigations

To pursue the goal, we initiated our studies using α-(trifluoromethyl) styrene **1a** and Ph_2SiH_2 **2a** as model substrates in the presence of Nickel catalysis (Table 1, for more details in Supplementary Table 1). The *anti*-Markovnikov addition product **3a** could be obtained in 18% yield by $Ni(cod)_2$ catalysis without the addition of any ligand (entry 1), and 17% yield with >20:1 L:B regioselectivity when PPh_3 was used as ligand at 30 °C (entry 2). Notably, altering the Ni/PPh_3 equivalent ratio from 1:2 to 1:1 resulted in a notable increase in the yield of **3a** to

https://doi.org/10.1038/s41467-024-50743-w

Table 1 | Optimization of reaction conditions[a]

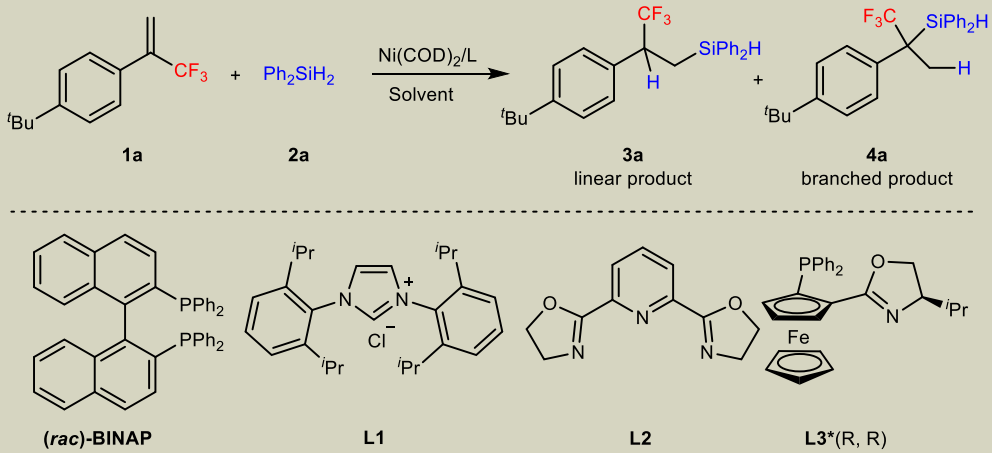

Entry	L	L (%)	Solvent	T/(°C)	Yield (%)	L:B (3a:4a)
1	—	—	toluene	30	18	>20:1
2	PPh_3	10 mol%	toluene	30	17	>20:1
3	PPh_3	5 mol%	toluene	30	96	>20:1
4	PCy_3	5 mol%	toluene	30	38	>20:1
5	BPY	5 mol%	toluene	30	<5	—
6	1,10-phen	5 mol%	toluene	30	<5	7:1
7[b]	**L1**	5 mol%	toluene	30	81	>20:1
8	**L2**	5 mol%	toluene	30	20	>20:1
9	**L3**	5 mol%	toluene	30	trace	—
10	BINAP	8 mol%	toluene	30	NR	—
11	BINAP	5 mol%	toluene	30	96	>1:20
12	BINAP	4.7 mol%	toluene	30	96	>1:20
13	BINAP	2.5 mol%	toluene	30	90	1:9
14	BINAP	5 mol%	DMA	30	trace	—
15	BINAP	5 mol%	MeO^{t}Bu	30	59	>1:20
16	BINAP	5 mol%	dioxane	30	95	>1:20
17	BINAP	5 mol%	DCE	30	NR	—
18	BINAP	5 mol%	THF	30	<5	—
19	BINAP	5 mol%	EtOH	30	NR	—
20	BINAP	5 mol%	toluene	0	NR	—
21[c]	BINAP	5 mol%	toluene	30	60	>1:20
22[c]	PPh_3	5 mol%	toluene	30	81	>20:1

[a]Reaction conditions: **1a** (0.2 mmol), **2a** (0.4 mmol), $Ni(cod)_2$ (5 mol%), **L** (x mol%), 30 °C in solvent (2.0 mL) under argon, 24 h, L:B value was determined by ^{19}F NMR, isolated yield.
[b]CsOAc (20 mol%).
[c]**2a** (0.2 mmol).

96% with >20:1 L:B value (entry 3). This 1:1 ratio might be beneficial for the generation of a highly reactive nickel catalyst. We then investigated other commercial available ligands (such as PCy_3, Bpy, 1, 10-phenanthroline, **L1**, **L2**, and **L3**), and found that all of these ligands gave anti-Markovnikov addition product **3a** or the recovery of starting materials (entries 4–9). Noteworthy, when bidentate phosphine ligand BINAP was used, the more challenging Markovnikov product **4a** was obtained with >20:1 B:L regioselectivity, and no by-products from β-F elimination were observed in the process (entries 10–13). The amount of BINAP in the system was significantly important for the efficiency, and **4a** could be obtained in 96% yield with >20:1 B:L ratio (entry 11). When the equivalent of BINAP ligand was slightly lower than Nickel, higher efficiency was observed (entry 12), indicating the equivalent of BINAP is significant for maintaining high efficiency with an appropriate Nickel:BINAP ratio. This emphasizes the importance of optimal balance for generating an efficiently active nickel catalyst. Then, we tested the solvent effect, and found that toluene gave the best result (entries 14–19). The ee of **4a** could be obtained in 45% value when chiral ligand (R)-BINAP was used under the reaction conditions of entry 11. Some other chiral ligands and solvent effects were also tested, but no better result was obtained (for more details in Supplementary Table 2). Low temperature and one equivalent of Ph_2SiH_2 led to diminished yield of desired products (entries 20–22). Control experiments showed that the nickel catalysis were essential for the transformation under the conditions of entry 3 or entry 11 (Supplementary Table 1 for details).

Substrates scope studies

With the optimized reaction conditions in hand, we next explored the substrate scope of this regiodivergent hydrosilylation reaction. The formation of *anti*-Markovnikov addition products were investigated first (Fig. 2). A variety of α-(trifluoromethyl)styrenes bearing functional groups such as electron-donating, electron-withdrawing and halide substituents at the *para*-position of the benzene ring, giving consistently products in 96–99% yield (**3a-3h**, L:B 7:1 to L:B > 20:1). The reaction can also tolerate reactive groups such as esters (**3i**, 99% yield and **3ii**, 89% yield), amine (**3j**, 54% yield) and triflate (**3k**, 42% yield). Other reduction-sensitive functional groups, such as aldehydes, ketones, and imines were not compatible for this hydrosilylation. These *meta*- substituted α-(trifluoromethyl)styrenes gave the corresponding products in excellent yield with excellent regioselectivity (**3l**, 94% yield, L:B 17:1 and **3 m**, 57% yield, L:B > 20:1). The *ortho*-substituted alkene gave lower yield of the desired product (**3n**, 40% yield, L:B > 20:1), potentially attributed to steric effect. Other (hetero)aryl-substituted and biaryl alkenes gave the corresponding products **3o-3t** in 96–99% yield. The structure of **3 s** was confirmed by X-ray crystallography (CCDC 2214736). The NHC ligand **L1** was employed for the electron-rich (hetero)aryl-substituted alkenes to give linear products **3u-3x** in 56–99% yield and excellent regioselectivity. Pleasingly, the N-heterocycles containing alkenes such as quinoline and indole also reacted smoothly to provide corresponding products (**3y**, 55% yield, L:B = 9:1 and **3z**, 89% yield, L:B = 18:1). High activity was realized for most substrates. Other fluoroalkyl groups (perfluoroethyl, perfluoropropyl, and difluoroethyl) substituted alkenes also underwent this hydrosilylation to produce β-fluoroalkyl substituted silanes in accepted yield (**3aa-3ac**, 54–80% yield) and excellent regioselectivity (L:B > 20:1). The reaction also tolerated for $PhMeSiH_2$ and gave the anti-Markovnikov product **3ad** in 79% yield but with 1:1 *dr* ratio of the relative stereochemistry between CF_3-containing carbon and Si center. However, the reaction of (3-(trifluoromethyl)but-3-en-1-yl)benzene, Ph_3SiH, $PhSiH_3$ all failed to give the desired product and starting materials were recovered even at elevated temperature.

We then explored the generality of the more challenging Markovnikov addition product systems. The substrate scope was found to be broad. As shown in Fig. 3, the reaction exhibited compatibility with various functional groups at the *para*-position of the benzene ring and gave the tetrasubstituted saturated silanes with excellent regioselectivity (**4a-4h**, 86–99% yield, B:L > 20:1). The reduction-sensitive functional groups such as aldehydes, ketones, imines, and amines proved to be incompatible. The hydrosilylation of alkene **1ii**, featuring with a carboxylic ester substituent at the benzene ring, resulted in a low yield of the desired product (**4ii**). For the triflate-substituted alkenes, the desired hydrosilylation product **4k** was obtained in 38% yield. The *meta*-substituted substrate also worked smoothly (**4l**, 99% yield, B:L > 20:1 and **4m**, 31% yield, B:L = 9:1), while the *ortho*-substituted alkene with a methyl group led to the recovery of starting materials (**4n**), even at elevated temperature due to steric effect. Other (hetero) aryl-substituted and biaryl α-(trifluoromethyl)styrenes were also tolerated, giving the corresponding products in excellent yield and regioselectivity (**4o-4u**, 83–99% yield, B:L 5:1 to B:L > 20:1). The structure of **4t** was confirmed by X-ray crystallography (CCDC 2214737). Other (hetero)aryl-substituted alkenes such as furan, thiophene, and indole were also compatible (**4v**, 54% yield, **4x**, 56% yield, and **4z**, 45% yield). We also briefly investigated alkenes with other fluoroalkyl substituents instead of CF_3 group (**4aa**, 46% yield, B:L > 20:1 and **4ab**, 40% yield, B:L > 20:1). The reaction of $PhMeSiH_2$ gave the hydrosilylation product, but with poor *regio*- and diastereoselectivity (**4ad**, 51% yield, B:L (**4ad**:**3ad**) = 1:2.3, dr (**3ad**) = 1:1, dr (**4ad**) = 1:1). The (3-(trifluoromethyl)but-3-en-1-yl)benzene, Ph_3SiH and $PhSiH_3$ failed to give the Markovnikov addition products.

Synthetic applications

The CF_3-containing silane products from this divergent hydrosilylation could undergo a series of transformations (Fig. 4). These reactions were successfully scaled up to 2.0 mmol without the erosion of yield and selectivity under reaction conditions A or conditions B (Fig. 4A). The *gem*-difluoroalkenes are useful synthetic intermediates and present interesting bioactive properties[67]. When TBAF was employed, the silane **4r** could be easily transformed into the *gem*-difluoroalkene **5**. The silane **3r** could be oxidized to alcohol **6** in 89% yield through the Fleming-Tamao oxidation process. Additionally, the silane **4r** reacted with styrene through the dehydrogenative process to give product **7** in 75% yield, and oxidized to monohydroxysilane **8** in 85% yield. The visible-light-mediated C–Si bond cleavage for the conjugate addition of **4r** with activated alkenes was realized, yielding the valuable CF_3-containing products with a quaternary carbon center (**9**, 54% yield and **10**, 56% yield) (Fig. 4B).

Mechanistic studies

We then performed several experiments to gain some insights into this regiodivergent hydrosilylation reaction mechanism (Fig. 5). The addition of 1, 1-diphenylethylene or BHT did not affect the yield and regioselectivity either under conditions A or conditions B. These results indicated a Chalk-Harrod reaction pathway rather than a radical pathway (Fig. 5A). EPR experiments also support these findings (for more details in Supplementary Figs. 19–22). When the CF_3 group was replaced by the Me or ^{i}Pr group, only linear product (**11** or **12**) was obtained no matter under the reaction conditions A or conditions B. These results indicated the trifluoromethyl group serves as a unique σ-electron-withdrawing group and is crucial to regioselectivity for the formation of Markovnikov products **4** (Fig. 5B). Moreover, the cyclopropyl-containing alkene gave the ring-opening product **13** under the conditions A. This regioselectivity is contrary to Me or ^{i}Pr group substituted alkenes, probably due to the favorable β-C elimination of cyclopropyl substituent, indicating the reversible NiH insertion and β-H elimination (Fig. 5B). The formation of product **13** suggested the NiH insertion pathway rather than the Ni–Si insertion pathway. The deuterium-labeling experiments were performed to investigate the source of hydrogen using the deuterated silane Ph_2SiD_2. The

https://doi.org/10.1038/s41467-024-50743-w

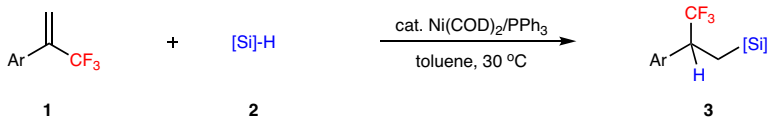

1 2 3

	R	yield	L:B
3a	^{t}Bu	99%	>20:1
3b	H	99%	>20:1
3c	^{i}Pr	99%	>20:1
3d	Me	99%	>20:1
3e	OMe	96%	>20:1
3f	CF_3	99%	9:1
3g	OCF_3	99%	7:1
3h	Cl	99%	>20:1
3i	COOMe	99%	>20:1
3ii	COO^{t}Bu	89%	>20:1

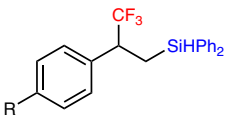

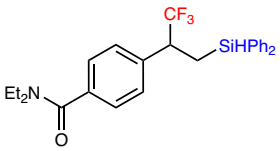

3j[b], 54% yield, L:B > 20:1

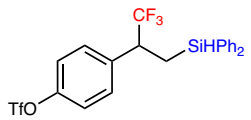

3k[b], 42% yield, L:B > 20:1

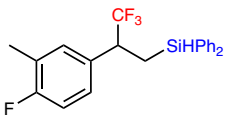

3l, 94% yield, L:B = 17:1

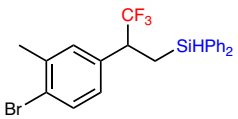

3m, 57% yield, L:B > 20:1

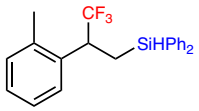

3n[b], 40% yield, L:B >20:1

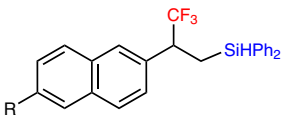

3o, R = H, 98% yield, L:B > 20:1
3p, R = OMe, 96% yield, L:B > 20:1
3q, R = OEt, 99% yield, L:B > 20:1

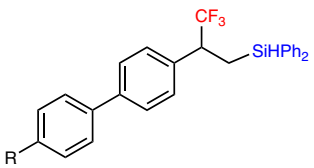

3r, R = H, 99% yield, L:B > 20:1
3s, R = Me, 99% yield, L:B > 20:1
CCDC 2214736 of **3s**

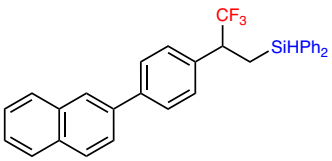

3t, 99% yield, L:B > 20:1

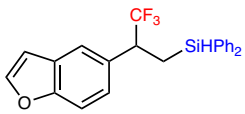

3u[c], 99% yield, L:B > 20:1

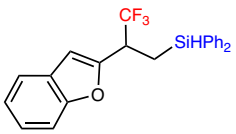

3v[c], 78% yield, L:B > 20:1

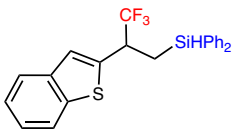

3w[c], 56% yield, L:B > 20:1

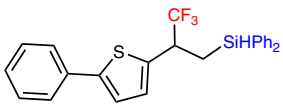

3x[c], 56% yield, L:B > 20:1

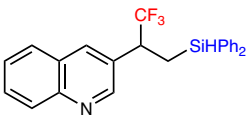

3y, 55% yield, L:B = 9:1

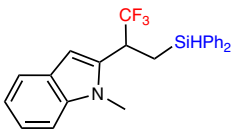

3z, 89% yield, L:B = 18:1

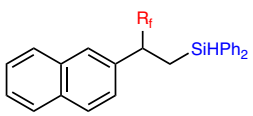

3aa, $R_f = C_2F_5$, 63% yield, L:B >20:1
3ab, $R_f = C_3F_7$, 54% yield, L:B >20:1

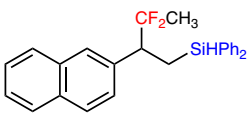

3ac, 80% yield, L:B > 20:1

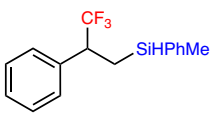

3ad, 79% yield, L:B > 20:1
dr = 1:1

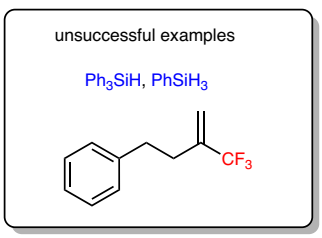

Fig. 2 | Substrate scope for β-fluoroalkyl substituted silanes. [a] Reaction conditions **A**: [a] **1** (0.2 mmol), [Si]-H **2** (0.4 mmol), $Ni(cod)_2$ (5 mol%), PPh_3 (5 mol%), 30 °C, in toluene (2.0 mL) under argon, 24 h, L:B value was determined by ^{19}F NMR, isolated yield. [b] 60 °C. [c] **L1** (5 mol%) and CsOAc (20 mol%) were used instead of PPh_3.

deuterated product **3d-d$_n$** was obtained under the Reaction conditions **A**, showing the H/D exchanged for proton in the alkene with that in Ph_2SiD_2 (Fig. 5C). These results indicate that the Ni-D species (from Ph_2SiD_2) inserted into the alkene **1d** and then β-H elimination gave NiH species when PPh_3 was used as ligand. While, when BINAP was used as a ligand, the deuterated product **4d-d$_n$** was obtained under the Reaction conditions **B** with 93% deuterium incorporation at the silicon atom, and only 8% H/D exchange occurred in the methyl group. This result indicates that the β-H elimination process is unlikely to proceed with the BINAP ligand. In addition, the parallel KIE studies with BINAP ligand revealed a KIE value of 1.1, suggesting the Si–H bond cleavage is not the turn-over limiting step (Fig. 5D). While, when PPh_3 was used as ligand,

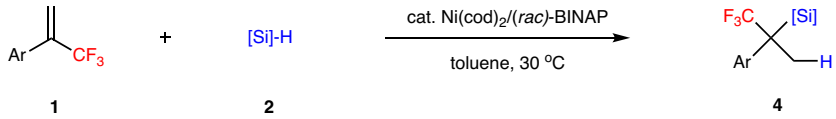

	R	yield	B:L (4:3)
4a	^{t}Bu	96%	> 20:1
4b^b	H	99%	> 20:1
4c	^{i}Pr	86%	> 20:1
4d	Me	97%	> 20:1
4e	OMe	96%	> 20:1
4f	CF_3	94%	> 20:1
4g	OCF_3	95%	> 20:1
4h^b	Cl	97%	> 20:1
4ii	COO^tBu	< 10%	--

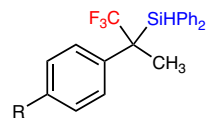

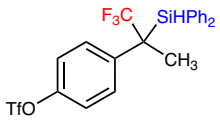

4k^{b,c}, 38% yield, B:L > 20:1

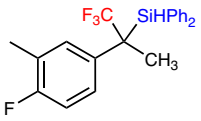

4l^b, 99% yield, B:L > 20:1

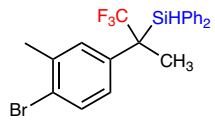

4m^{b,c}, 31% yield, B:L = 9:1

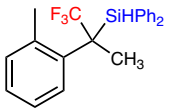

4n, NR

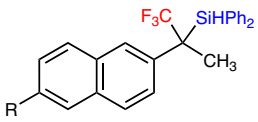

4o^b, R = H, 99% yield, B:L > 20:1
4p^b, R = OMe, 99% yield, B:L > 20:1
4q^b, R = OEt, 99% yield, B:L > 20:1

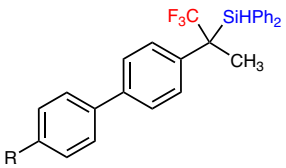

4r^b, R = H, 99% yield, B:L > 20:1
4s^b, R = Me, 95% yield, B:L > 20:1

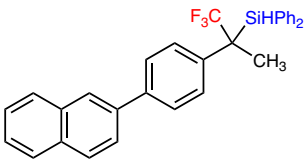

4t, 99% yield, B:L > 20:1
CCDC 2214737

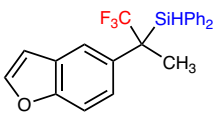

4u^b, 83% yield, B:L = 5:1

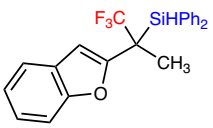

4v, 54% yield, B:L = 7:1

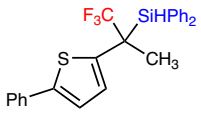

4x^b, 56% yield, B:L > 20:1

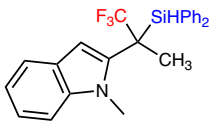

4z^{b,c}, 45% yield, B:L = 7:1

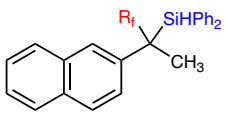

4aa, $R_f = C_2F_5$, 46% yield, B:L > 20:1
4ab, $R_f = C_3F_7$, 40% yield, B:L > 20:1

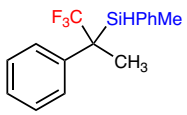

4ad^{b,c},51% yield, B:L = 1:2.3
dr of **3ad** =1:1, dr of **4ad** = 1:1

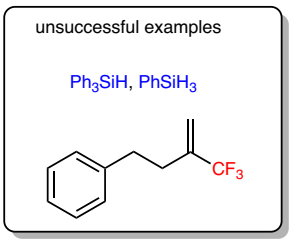

Fig. 3 | Substrate scope for α-fluoroalkyl substituted silanes. [a]Reaction conditions **B**: [a] **1** (0.2 mmol), **2** (0.4 mmol), $Ni(cod)_2$ (5 mol%), *rac*-BINAP (5.0 mol%), 30 °C, solvent (2.0 mL), argon, 24 h, L:B value was determined by ^{19}F NMR, isolated yield. [b] *rac*-BINAP (4.7 mol%). [c] 60 °C.

an unexpected inverse kinetic isotope effect was observed (KIE = 0.4), probably resulting from the generation of **1r-d**. These results indicate that the NiH insertion and β-H elimination processes occur before the C–Si bond formation.

DFT studies

To elucidate the origin of this unexpectedly excellent regioselectivity in the hydrosilylation of fluoroalkyl-alkenes[51–54,68]. we performed the density functional theory (DFT) calculations (Figs. 6, 7). We first investigated the detailed mechanism of Ni/BINAP system, which delivered the more challenging Markovnikov product. As shown in Fig. 6, the BINAP-bound-Ni(0) species **INT1** was set to the relative zero energy. The Ni(0) species undergo oxidative addition of [Si]–H through the transition state **TS1**, with a calculated free energy barrier of 1.1 kcal mol^{-1}. This process results in the formation of intermediate **INT2** with a slight exergonicity of 4.6 kcal mol^{-1}. Then, the α-(trifluoromethyl)styrene **1b** coordinates to the NiH species **INT2** and undergoes [1, 2]-insertion, giving intermediate **INT4** through the transition state **TS3** with an activation barrier of 16.8 kcal mol^{-1}. Alternatively, the NiH [2, 1]-insertion results in the formation of intermediate **INT3** through the transition state **TS2** with a higher activation barrier of 22.8 kcal mol^{-1}. The lower energy barrier observed in the [1, 2]-insertion compared to [2, 1]-insertion is attributed to the σ-withdrawing effect of the trifluoromethyl group.

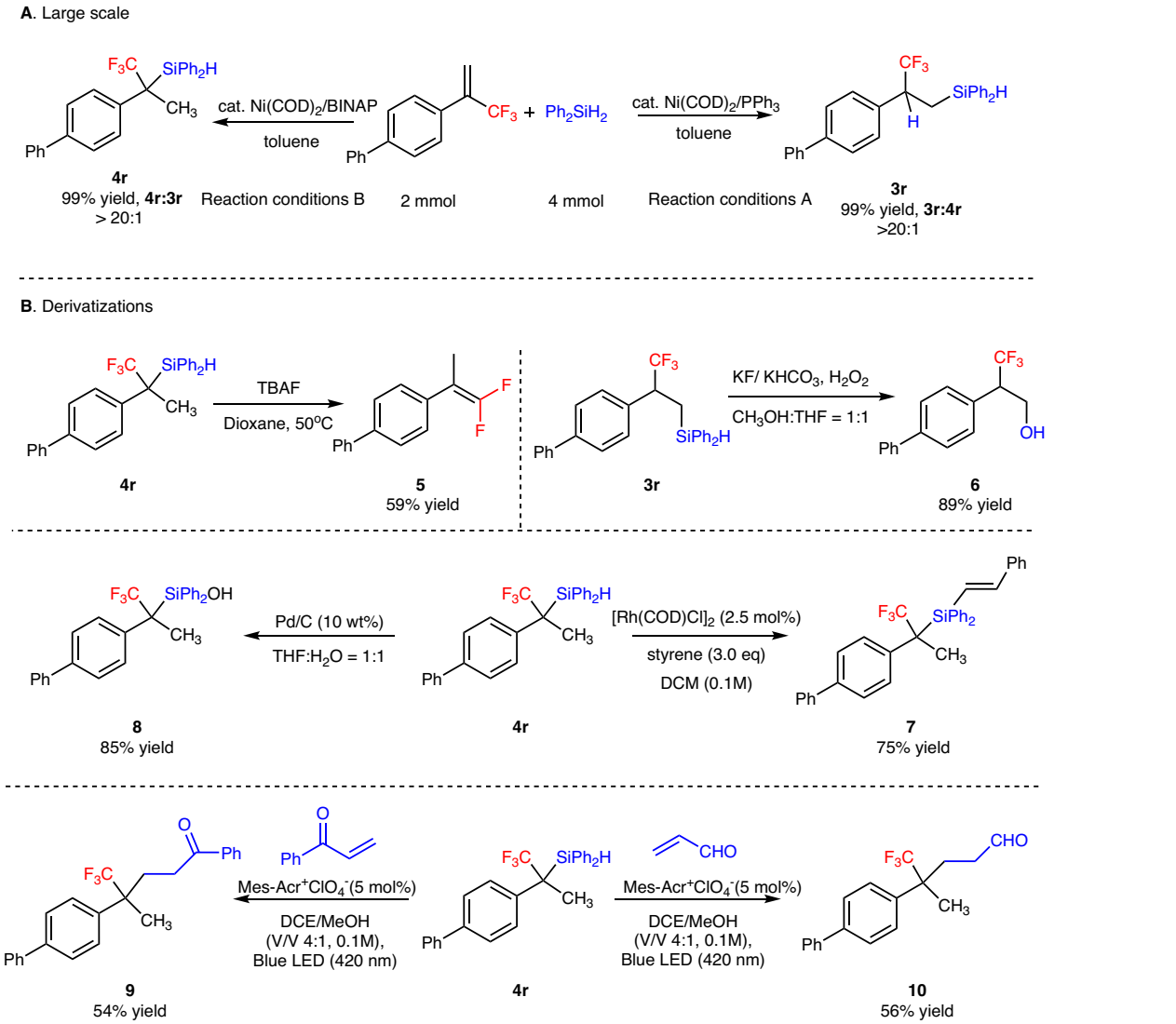

Fig. 4 | Scale-up reaction and derivatization. A Large scale experiments. **B** Derivatizations.

The subsequent C(sp^3)–Si reductive elimination from intermediate **INT4** occurs through the transition state **TS4**, resulting in an overall activation-free energy barrier of 29.2 kcal mol^{-1}. After detailed investigation, we found that the open-shell singlet species **INT4-oss** through spin-state changes from closed-shell singlet species **INT4** would undergo a lower overall activation barrier of 20.7 kcal mol^{-1} *via* transition state **TS4-oss** (which is lower than **TS2**). Finally, ligand exchange with Ph_2SiH_2 **2a** release the Markovnikov product **3b** and the active catalytic species **INT1** to complete the catalytic cycle. This unique open-shell singlet reaction mechanism is attributed to the d-d orbital transformation in the nickel center[69] and steric repulsion between BINAP with the trifluoromethyl group[70].

Subsequently, a DFT calculation was elucidated on the reaction mechanism of the Ni/PPh_3 system. As shown in Fig. 7, the monodentate phosphine ligand PPh_3 bound-Ni(0) species **INT5** was set to the relative zero energy. The oxidative addition of [Si]–H to the nickel center *via* transition state **TS5** with a low energy barrier of 4.0 kcal mol^{-1}, giving the intermediate **INT6**. The α-(trifluoromethyl) styrene **1b** coordinates to the nickel center and gives **INT7**, which undergoes [2, 1]-insertion to give the intermediate **INT8** through transition state **TS6** with an activation barrier of 1.4 kcal mol^{-1}. The following C(sp^3)–Si reductive elimination from intermediate **INT8** occurs through transition state **TS7** with a very low energy barrier of 1.8 kcal mol^{-1}. This process lead to the formation of the final anti-Markovnikov product **3b** and the regeneration of active catalytic species **INT5** through the coordination of another Ph_2SiH_2 **2a**. Alternatively, the Ni-H undergoes [1, 2]-insertion resulting in the formation of intermediate **INT9** through transition state **TS6'**. However, the subsequent C(sp^3)–Si reductive elimination from **INT9** via transition state **TS8** exhibits a high energy barrier of 18.5 kcal mol^{-1}. The high selectivity of the generation of anti-Markovnikov product can be attributed to the elevated energy barrier for C(sp^3)–Si reductive elimination energy barrier. DFT calculations of the open-shell singlet transition state **TS8-oss** reveal that the energy barrier for C(sp^3)–Si reductive elimination in Ni/PPh_3 system does not decrease but increase to 30.5 kcal mol^{-1}. We also exclude the reaction pathway with two PPh_3 ligand bound-Ni(0) species (for more details in Supplementary Fig. 40, and entry 2 vs 3 in Table 1). These DFT calculation results are also consistent with our experimental results.

In summary, we have developed ligand-controlled regiodivergent nickel(0)-catalyzed hydrosilylation of α-(fluoroalkyl)styrenes for the direct generation of fluoroalkyl-containing silanes in good to excellent yield. This approach provides a versatile platform for the selective formation of both α-trifluoromethylsilanes and β-trifluoromethylsilanes, utilizing only two readily available ligands.

https://doi.org/10.1038/s41467-024-50743-w

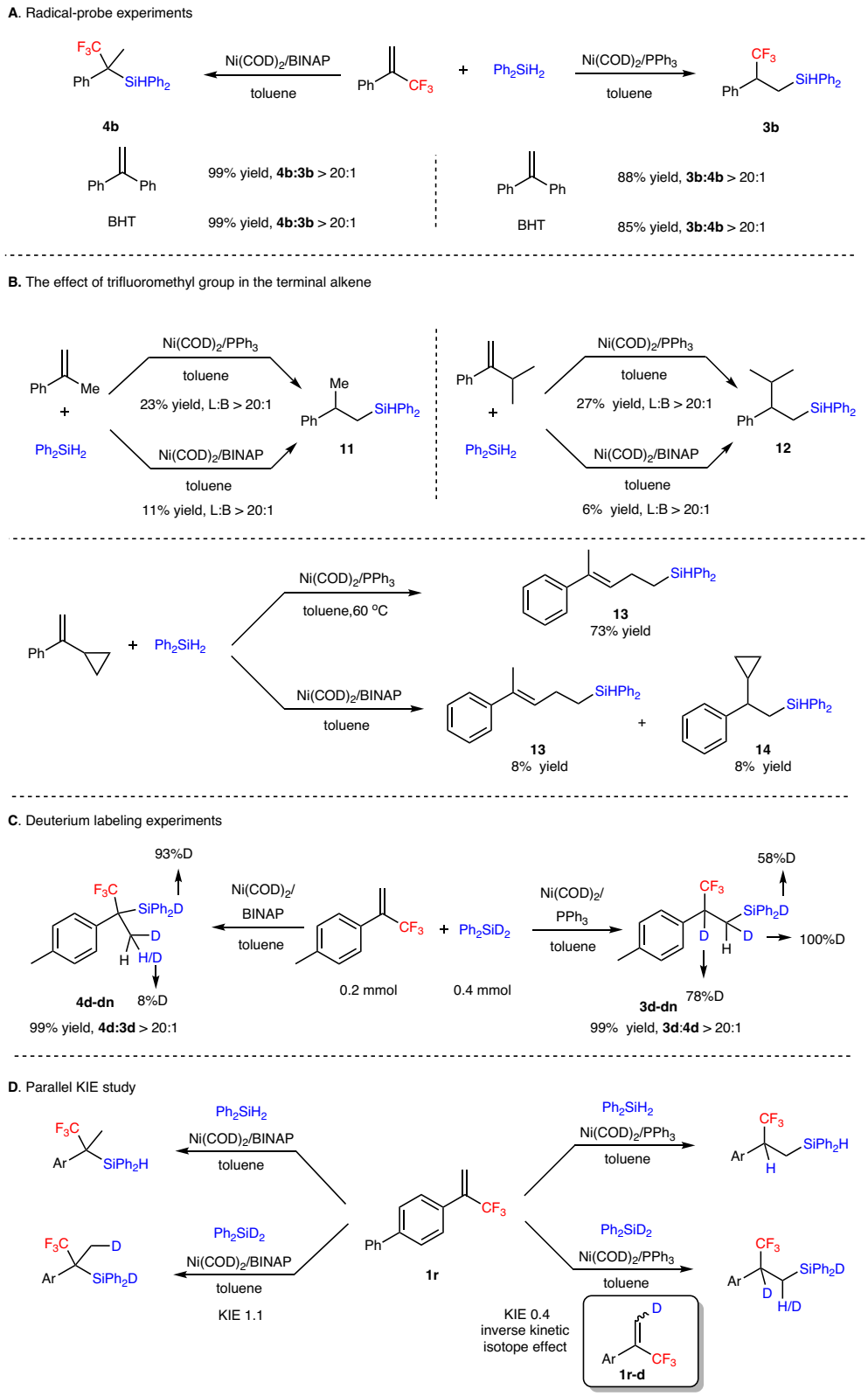

Fig. 5 | Mechanistic studies. A Radical-probe experiments. **B** The effect of trifluoromethyl group in the terminal alkene. **C** Deuterium-labeling experiments. **D** Parallel KIE studies.

https://doi.org/10.1038/s41467-024-50743-w

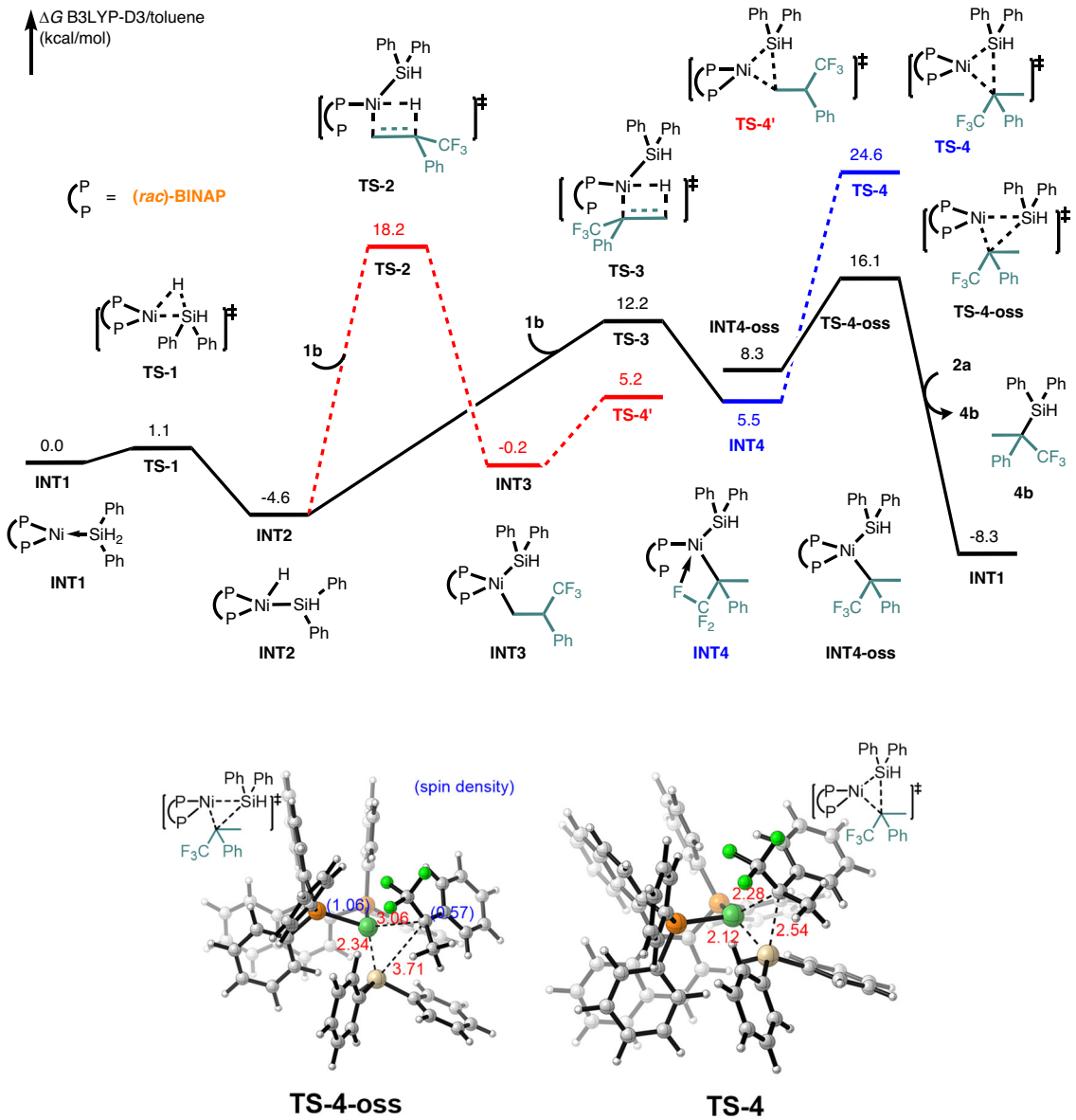

Fig. 6 | DFT Studies for Markovnikov product 4. DFT calculation for the Ni/BINAP system to generate Markovnikov product **4**.

Mechanistic studies, including DFT calculations, have revealed that the trifluoromethyl group and the structure of the ligand significantly influence the regioselectivity. The distinctive spin-state changes from closed-shell singlet species to open-shell singlet are believed to form unusual tetrasubstituted saturated Markovnikov products. This study contributed to the rapid and divergent synthesis of $C(sp^3)–R_f$ (R_f = fluoroalkyl) containing compounds, and provided insights for further development of regio-controlled hydrosilylation involving steric hindrance alkenes.

Methods

General procedure for the generation of *anti*-Markovnikov addition product 3

General procedure A: $Ni(cod)_2$ (2.8 mg, 0.01 mmol) and PPh_3 (2.6 mg, 0.01 mmol) in toluene (2.0 mL) were charged into a 25 mL pressure tube under argon. The mixture was stirred for 30 min at room temperature, followed by the addition of Ph_2SiH_2 (78 mg, 0.4 mmol), after stirred for 20 min, α-(fluoroalkyl)styrenes **1** (0.2 mmol, 1.0 equiv) was added to the reaction mixture. The reaction tube was then sealed and placed in an oil bath at 30 °C. After stirred for 24 h, the reaction mixture was filtered through a pad of celite, eluted with ethyl acetate, concentrated and purified by silica gel chromatography (PE) to give the indicated product **3**.

General procedure for the generation of Markovnikov addition product 4

General procedure B: $Ni(cod)_2$ (2.8 mg, 0.01 mmol) and *rac*-BINAP (6.2 mg, 0.01 mmol) in toluene (2.0 mL) were charged into a 25 mL pressure tube under argon. The mixture was stirred for 30 min at room temperature, followed by addition of Ph_2SiH_2 (78 mg, 0.4 mmol), after stirred for 20 min, α-(fluoroalkyl)styrenes **1** (0.2 mmol, 1.0 equiv) was added to the reaction mixture. The reaction tube was then sealed and placed in an oil bath at 30 °C. After stirred for 24 h, the reaction mixture was filtered through a pad of celite, eluted with ethyl acetate, concentrated and purified by silica gel chromatography (PE) to give the indicated product **4**.

More details and characterization of the products are available in Supplementary Information.

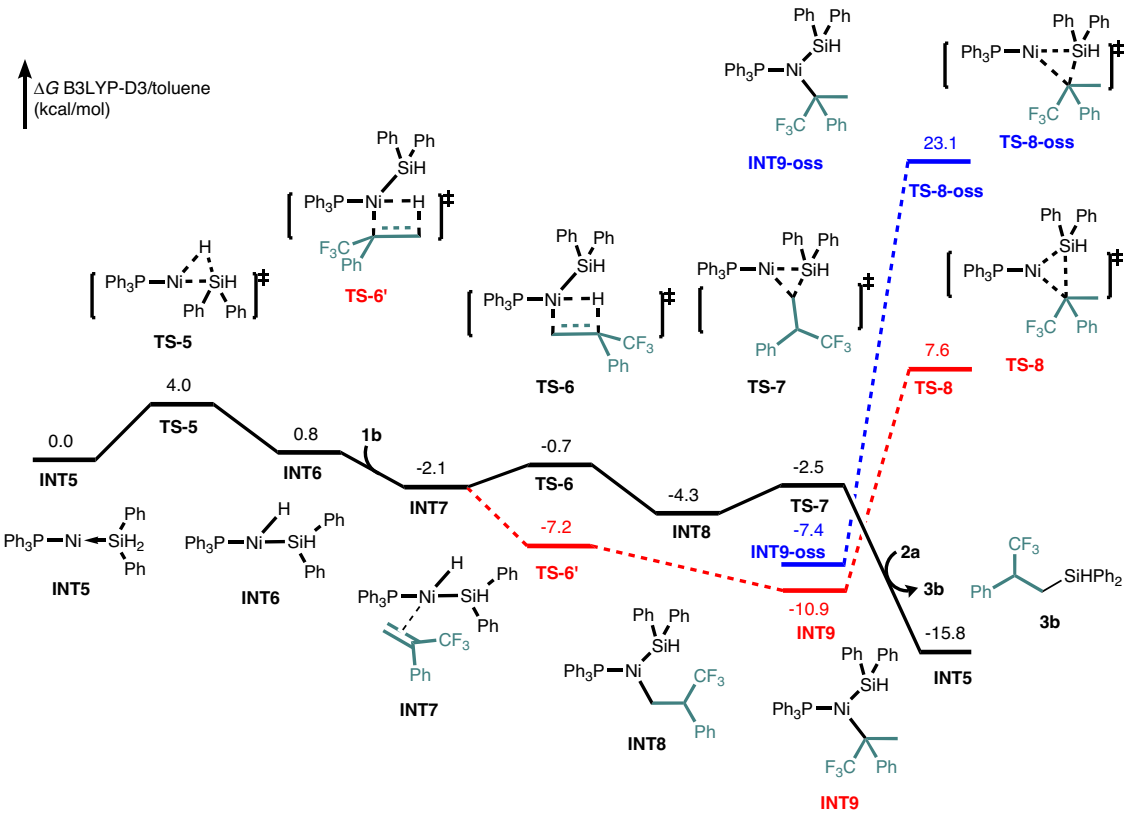

Fig. 7 | DFT Studies for anti-Markovnikov product 3. DFT calculations for the Ni/PPh_3 system to generate anti-Markovnikov product **3**.

Data availability

The authors declare that the data supporting the findings of this study are available within the paper and its Supplementary Information files, and also available from the corresponding author. The NMR, experimental procedures and characterization for all products and mechanism studies are shown in Supplementary Information files. Crystallographic data for the structures reported in this Article have been deposited at the Cambridge Crystallographic Data Centre, under deposition numbers CCDC 2214736 (**3 s**), CCDC 2214737 (**4t**). Copies of the data can be obtained free of charge via https://www.ccdc.cam.ac.uk/structures/. Source data are provided with this paper.

References

1. Müller, K., Faeh, C. & Diederich, F. Fluorine in pharmaceuticals: looking beyond intuition. *Science* **317**, 1881–1886 (2007).
2. Purser, S., Moore, P. R., Swallow, S. & Gouverneur, V. Fluorine in medicinal chemistry. *Chem. Soc. Rev.* **37**, 320–330 (2008).
3. Kirsch, P. *Modern Fluoroorganic Chemistry: Synthesis Reactivity, Applications*. 2nd edn (Wiley-VCH, 2013).
4. Wang, J. et al. Fluorine in pharmaceutical industry: fluorine-containing drugs introduced to the market in the last decade (2001–2011). *Chem. Rev.* **114**, 2432–2506 (2014).
5. Meanwell, N. A. Fluorine and fluorinated motifs in the design and application of biosisosteres for drug design. *J. Med. Chem.* **61**, 5822–5880 (2018).
6. Mei, H. B. et al. Fluorine-containing drugs approved by the FDA in 2019. *Chin. Chem. Lett.* **31**, 2401–2413 (2020).
7. Chu, L. L. & Qing, F. L. Copper-mediated arobic oxidative trifluoromethylation of terminal alkynes with Me_3SiCF_3. *J. Am. Chem. Soc.* **132**, 7262–7263 (2010).
8. Liang, T., Neumann, C. N. & Ritter, T. Introduction of fluorine and fluorine-containing functional groups. *Angew. Chem. Int. Ed.* **52**, 8214–8264 (2013).
9. Alonso, C., Marigorta, E. M., Rubiales, G. & Palacios, F. Carbon trifluoromethylation reactions of hydrocarbon derivatives and heteroarenes. *Chem. Rev.* **115**, 1847–1935 (2015).
10. Liu, X., Xu, C., Wang, M. & Liu, Q. Trifluoromethyltrimethylsilane: nucleophilic trifluoromethylation and beyond. *Chem. Rev.* **115**, 683–730 (2015).
11. Feng, Z., Xiao, Y. L. & Zhang, X. Transition-metal (Cu, Pd, Ni)-catalyzed difluoroalkylation via cross-coupling with difluoroalkylhalides. *Acc. Chem. Res.* **51**, 2264–2278 (2018).
12. Ni, C. F., Hu, M. Y. & Hu, J. B. Good partnership between sulfur and fluorine: sulfur-based fluorination and fluoroalkylation reagents for organic synthesis. *Chem. Rev.* **115**, 765–825 (2015).
13. Yang, X., Wu, T., Phipps, R. J. & Toste, F. D. Advances in catalytic enantioselective fluorination, mono-, di-, and trifluoromethylation, and trifluoromethylthiolation reactions. *Chem. Rev.* **115**, 826–870 (2015).
14. Qing, F. L. et al. A fruitful decade of organofluorine chemistry: new reagents and reactions. *CCS Chem.* **4**, 2518–2549 (2022).
15. Zhang, C. P. et al. Copper-mediated trifluoromethylation of heteroaromatic compounds by trifluoromethyl sulfonium salts. *Angew. Chem. Int. Ed.* **50**, 1896–1900 (2011).
16. Bai, D. C., Wang, X. L., Zheng, G. F. & Li, X. W. Redox-divergent synthesis of fluoroalkylated pyridines and 2-pyridones through Cu-catalyzed N-O cleavage of oxime acetates. *Angew. Chem. Int. Ed.* **57**, 6633–6637 (2018).
17. Wang, X. et al. Controllable single and double difluoromethylene insertions into C-Cu bonds: copper-mediated tetrafluoroethylation and hexafluoropropylation of aryl iodides with $TMSCF_2H$ and $TMSCF_2Br$. *J. Am. Chem. Soc.* **144**, 12202–12211 (2022).
18. Hu, M., Ni, C. & Hu, J. Copper-mediated trifluoromethylation of α-diazo esters with $TMSCF_3$: the important role of water as a promoter. *J. Am. Chem. Soc.* **134**, 15257–15260 (2012).

19. Liang, Y. & Fu, G. C. Stereoconvergent Negishi arylations of racemic secondary alkyl electrophiles: differentiating between a CF_3 and an alkyl group. *J. Am. Chem. Soc.* **137**, 9523–9526 (2015).
20. Huang, W., Hu, M., Wan, X. & Shen, Q. Facilitating the transmetalation step with aryl-zincates in nickel-catalyzed enantioselective arylation of secondary benzylic halides. *J. Am. Chem. Soc.* **141**, 11446–11451 (2019).
21. Lin, T. Y. et al. Design and synthesis of TY-phos and application in palladium-catalyzed enantioselective fluoroarylation of gem-difluoroalkenes. *Angew. Chem. Int. Ed.* **59**, 22957–22962 (2020).
22. Huang, S. et al. Regio- and enantioselective umpolung gemdifluoroallylation of hydrazones via palladium catalysis enabled by N-heterocyclic carbene ligand. *Nat. Commun.* **12**, 6551 (2021).
23. Bai, D. C. et al. Highly regio- and enantioselective hydrosilylation of gem-difluoroalkenes by nickel catalysis. *Angew. Chem. Int. Ed.* **61**, e202114918 (2022).
24. Tian, F. T., Yan, G. B. & Yu, J. Recent advances in the synthesis and applications of α-(trifluoromethyl)styrenes in organic synthesis. *Chem. Commun.* **55**, 13486–13505 (2019).
25. Lu, X. et al. Nickel-catalyzed allylic defluorinative alkylation of trifluoromethyl alkenes with reductive decarboxylation of redox-active esters. *Chem. Sci.* **10**, 809–814 (2019).
26. Chen, F. L., Xu, X. F., He, Y. L., Huang, G. P. & Zhu, S. L. NiH-catalyzed migratory defluorinative olefin cross-coupling: trifluoromethyl-substituted alkenes as acceptor olefins to form gem-difluoroalkenes. *Angew. Chem. Int. Ed.* **59**, 5398–5402 (2020).
27. Deng, Y. P., He, J. J., Cao, S. & Qian, X. H. Advances in cycloaddition and hydroaddition reaction of α-(trifluoromethyl)styrenes without defluorination: an alternative approach to CF_3-containing compounds. *Chin. Chem. Lett.* **33**, 2363–2371 (2022).
28. Huang, W. S. et al. General catalytic enantioselective access to monohalomethyl and trifluoromethyl cyclopropanes. *Chem. Eur. J.* **24**, 10339–10343 (2018).
29. Hock, K. J., Spitzner, R. & Koenigs, R. M. Towards nitrile-substituted cyclopropanes – a slow-release protocol for safe and scalable applications of diazo acetonitrile. *Green. Chem.* **19**, 2118–2122 (2017).
30. Trost, B. M. & Debien, L. Palladium-catalyzed trimethylenemethane cycloaddition of olefins activated by the σ-electron-withdrawing trifluoromethyl group. *J. Am. Chem. Soc.* **137**, 11606–11609 (2015).
31. Magre, M., Biosca, M., Pámies, O. & Diéguez, M. Filling the gaps in the challenging asymmetric hydroboration of 1,1-disubstituted alkenes with simple phosphite-based phosphinooxazoline iridium catalysts. *Chem. Cat. Chem.* **7**, 114–120 (2015).
32. Hu, M., Tan, B. B. & Ge, S. Z. Enantioselective cobalt-catalyzed hydroboration of fluoroalkyl-substituted alkenes to access chiral fluoroalkylboronates. *J. Am. Chem. Soc.* **144**, 15333–15338 (2022).
33. Zhu, C. et al. Nickel-catalyzed anti-Markovnikov hydroalkylation of trifluoromethylalkenes. *ACS Catal.* **12**, 9410–9417 (2022).
34. Brook, M. A. *Silicon in Organic, Organometallic and Polymer Chemistry* (Wiley, 2000).
35. Pooni, P. K. & Showell, G. A. Silicon switches of marketed drugs. *Mini Rev. Med. Chem.* **6**, 1169–1177 (2006).
36. Xu, L. W., Li, L., Lai, G. Q. & Jiang, J. X. The recent synthesis and application of silicon-stereogenic silanes: a renewed and significant challenge in asymmetric synthesis. *Chem. Soc. Rev.* **40**, 1777–1790 (2011).
37. Franz, A. K. & Wilson, S. O. Organosilicon molecules with medicinal applications. *J. Med. Chem.* **56**, 388–405 (2013).
38. Bart, S. C., Lobkovsky, E. & Chirik, P. J. Preparation and molecular and electronic structures of iron(0) dinitrogen and silane complexes and their application to catalytic hydrogenation and hydrosilation. *J. Am. Chem. Soc.* **126**, 13794–13807 (2004).
39. Chen, J. H., Cheng, B., Cao, M. Y. & Lu, Z. Iron-catalyzed asymmetric hydrosilylation of 1,1-disubstitutedAlkenes. *Angew. Chem. Int. Ed.* **54**, 4661–4664 (2015).
40. Cheng, B., Liu, W. B. & Lu, Z. Iron-catalyzed highly enantioselective hydrosilylation of unactivated terminal alkenes. *J. Am. Chem. Soc.* **140**, 5014–5017 (2018).
41. Hu, M. Y. et al. Iron-catalyzed regiodivergent alkyne hydrosilylation. *J. Am. Chem. Soc.* **142**, 16894–16902 (2020).
42. Cheng, B., Lu, P., Zhang, H. Y., Cheng, X. P. & Lu, Z. Highly enantioselective cobalt-catalyzed hydrosilylation of alkenes. *J. Am. Chem. Soc.* **139**, 9439–9442 (2017).
43. Wang, C., Teo, W. J. & Ge, S. Z. Cobalt-catalyzed regiodivergent hydrosilylation of vinylarenes and aliphatic alkenes: ligand- and silane-dependent regioselectivities. *ACS Catal.* **7**, 855–863 (2017).
44. Wen, H. N., Wang, K., Zhang, Y. L., Liu, G. X. & Huang, Z. Cobalt-catalyzed regio- and enantioselective Markovnikov 1,2- hydrosilylation of conjugated dienes. *ACS Catal.* **9**, 1612–1618 (2019).
45. Lipschutz, M. I. & Tilley, T. D. Synthesis and reactivity of a conveniently prepared two-coordinate bis(amido) nickel(II) complex. *Chem. Commun.* **48**, 7146–7148 (2012).
46. Buslov, I., Becouse, J., Mazza, S., Montandon-Clerc, M. & Hu, X. Chemoselective alkene hydrosilylation catalyzed by nickel pincer complexes. *Angew. Chem. Int. Ed.* **54**, 14523–14526 (2015).
47. Steiman, T. J. & Uyeda, C. Reversible substrate activation and catalysis at an intact metal– metal bond using a redox-active supporting ligand. *J. Am. Chem. Soc.* **137**, 6104–6110 (2015).
48. Buslov, I., Keller, S. C. & Hu, X. L. Alkoxy hydrosilanes as surrogates of gaseous silanes for hydrosilylation of alkenes. *Org. Lett.* **18**, 1928–1931 (2016).
49. Pappas, I., Treacy, S. & Chirik, P. J. Alkene hydrosilylation using tertiary silanes with α-diimine nickel catalysts. Redox-active ligands promote a distinct mechanistic pathway from platinum catalysts. *ACS Catal.* **6**, 4105–4109 (2016).
50. Mathew, J. et al. Olefin hydrosilylation catalyzed by cationic nickel(ii) allyl complexes: a non-innocent allyl ligand-assisted mechanism. *Chem. Commun.* **52**, 6723–6726 (2016).
51. Corey, J. Y. Reactions of hydrosilanes with transition metal complexes and characterization of the products. *Chem. Rev.* **111**, 863–1071 (2011).
52. Nakajima, Y. & Shimada, S. Hydrosilylation reaction of olefins: recent advances and perspectives. *RSC Adv.* **5**, 20603–20616 (2015).
53. Du, X. Y. & Huang, Z. Advances in base-metal-catalyzed alkene hydrosilylation. *ACS Catal.* **7**, 1227–1243 (2017).
54. Sunada, Y. & Nagashima, H. in *Organosilicon Chemistry: Novel Approaches and Reactions* (eds Hiyama, T. & Oestreich, M.) (WileyVCH, 2019).
55. Gao, Y. F., Wang, L. J. & Deng, L. Distinct catalytic performance of cobalt(I)–N-heterocyclic carbene complexes in promoting the reaction of alkene with diphenylsilane: selective 2,1-hydrosilylation, 1,2-hydrosilylation, and hydrogenation of alkene. *ACS Catal.* **8**, 9637–9646 (2018).
56. Agahi, R. et al. Regiodivergent hydrosilylation, hydrogenation, [2π + 2π]-cycloaddition and C–H borylation using counterion activated earth-abundant metal catalysis. *Chem. Sci.* **10**, 5079–5084 (2019).
57. Kuai, C. S. et al. Ligand-regulated regiodivergent hydrosilylation of isoprene under iron catalysis. *Angew. Chem. Int. Ed.* **59**, 19115–19120 (2020).
58. Hossain, I. & Schmidt, J. A. Cationic nickel(II)-catalyzed hydrosilylation of alkenes: role of P, N-type ligand scaffold on selectivity and reactivity. *Organometallics* **39**, 3441–3451 (2020).
59. Wu, X. Y. et al. Nickel-catalyzed hydrosilylation of terminal alkenes with primary silanes via electrophilic silicon–hydrogen bond activation. *Org. Lett.* **23**, 1434–1439 (2021).

60. Docherty, J. H., Dominey, A. P. & Thomas, S. P. Cobalt-catalysed, ligand-controlled regiodivergent alkene hydrosilylation. *Asian J. Org. Chem.* **10**, 2379–2384 (2021).
61. Cheng, Z.-Y. et al. Cobalt-catalyzed regiodivergent double hydrosilylation of arylacetylenes. *Angew. Chem. Int. Ed.* **61**, e202215029 (2022).
62. Chen, Y. & Zargarian, D. Phenylsilane dehydrocoupling and addition to styrene catalyzed by (R-indenyl)Ni(phosphine)(methyl) complexes. *Can. J. Chem.* **87**, 280–287 (2009).
63. Junquera, L. B., Puerta, M. C. & Valerga, P. R-Allyl nickel(II) complexes with chelating N-heterocyclic carbenes: synthesis, structural characterization, and catalytic activity. *Organometallics* **31**, 2175–2183 (2012).
64. Yao, C. B., Wang, S., Norton, J. & Hammond, M. Catalyzing the hydrodefluorination of CF_3-substituted alkenes by $PhSiH_3$. H• transfer from a nickel hydride. *J. Am. Chem. Soc.* **142**, 4793–4799 (2020).
65. Bott, G., Field, L. D. & Sternhell, S. Steric effects. a study of a rationally designed system. *J. Am. Chem. Soc.* **102**, 5618–5626 (1980).
66. Furuya, T., Kamlet, A. S. & Ritter, T. Catalysis for fluorination and trifluoromethylation. *Nature* **473**, 470–477 (2011).
67. Meanwell, N. A. Synopsis of some recent tactical application of bioisosteres in drug design. *J. Med. Chem.* **54**, 2529–2591 (2011).
68. Chang, A. S. et al. (NHC)Ni(0)-catalyzed branched-selective alkene hydrosilylation with secondary and tertiary silanes. *ACS Catal.* **12**, 11002–11014 (2022).
69. Zhu, B. & Sakaki, S. C(sp3)–F bond activation and hydrodefluorination of the CF_3 group catalyzed by a nickel(II) hydride complex: theoretical insight into the mechanism with a spin-state change and two ion-pair intermediates. *ACS Catal.* **11**, 10681–10693 (2021).
70. Marciniec, B. Catalysis by transition metal complexes of alkene silylation – recent progress and mechanistic implications. *Coord. Chem. Rev.* **249**, 2374–2390 (2005).

Acknowledgements

This work is supported by the NSFC (Nos. 82130103 (J.C.), U1804283 (J.C.), 21801067 (D.B.)), the Central Plains Scholars and Scientists Studio Fund (2018002 (J.C.)), and the Project funded by the Natural Science Foundation of Henan (242300421351 (D.B.), 202300410225 (H.W.), 222102310562 (H.W.)) and Henan Postdoctoral Science Foundation (202103087 (H.W.)). We also thank the financial support from Henan Key Laboratory of Organic Functional Molecules and Drug Innovation.

Author contributions

D.B. initiated the project, designed and directed the project, completed product characterizations, and wrote the manuscript; L.C. and F.W. did some experiments and some analysis of products; K.Z. and Y.Q. did DFT calculation.; G.X., and J.C. supported the project and wrote the manuscript. J.C. also directed the project.

Competing interests

The authors declare no competing interests.

Additional information

Supplementary information The online version contains supplementary material available at https://doi.org/10.1038/s41467-024-50743-w.

Correspondence and requests for materials should be addressed to Dachang Bai or Junbiao Chang.

Peer review information *Nature Communications* thanks Genping Huang and the other anonymous reviewer(s) for their contribution to the peer review of this work. A peer review file is available.